PERGAMON

International Journal of Heat and Mass Transfer 43 (2000) 665–676

International Journal of HEAT and MASS TRANSFER

www.elsevier.com/locate/ijhmt

Revisiting the Reynolds-averaged energy equation in near-wall turbulence models

Keh-Chin Chang*, Ming-Juin Shyu

Department of Aeronautics and Astronautics, National Cheng-Kung University, Tainan 701, Taiwan

Received 8 October 1998; received in revised form 18 May 1999

Abstract

It is sometimes reported in the heat transfer studies of gaseous media using the near-wall turbulence models that their fully-developed *Nu* predictions deviate from the experimental correlations. This work approaches the rigorous formulation of the Reynolds-averaged equation in terms of temperature from a fundamental basis, in order to highlight the possible errors due to the usual overapproximation made for the Reynolds-averaged energy equation. It is suggested that Eq. (18) which is one of the rigorous forms of the Reynolds-averaged equation and free of the unknown correlation of the pressure diffusion term is suitable for the analysis of turbulent convective heat transfer in gaseous media.

Keywords: Turbulent heat transfer; Reynolds-averaged energy equation

1. Introduction

In a very recent paper (Hrenya et al. [1]), a comparative study of nine different versions of low Reynolds number (LRN) k–ε turbulence models in terms of their ability to predict wall heat transfer rates for straight pipe flow was carried out. Remarkable deviations (around 18%) in the Nusselt number predictions from the experimental correlations were found even when the algebraic expression of variable turbulent Prandtl number in terms of turbulent Peclet number, as proposed by Kays and Crawford [2], was applied to the calculations. Level of agreement of the predictions with the experimental correlations for a given turbulence model was attributed to the unique ability of this model to accurately capture the radial distribution of the eddy viscosity (μ_t) in the study of Hrenya et al. Similar observations were reported by Chang et al. [3] in the predictions of the fully developed Nusselt number for straight-pipe flows using four different versions of low Reynolds number k–ε models but with the assumption of constant turbulent Prandtl number, as compared to the experimental correlations.

The preceding analyses of turbulent heat transfer problems were to solve the Reynolds-averaged energy equation in which the turbulent heat flux was modeled by using the classical Boussinesq approximation,

$$\overline{-u_j'\theta'} = \alpha_t \frac{\partial \theta}{\partial x_j} \tag{1}$$

The unknown eddy diffusivity for heat α_t, is expressed by the known eddy viscosity so that

$$\alpha_t = \frac{\nu_t}{\sigma_t} \tag{2}$$

Thus, in this formulation the analogy is assumed

* Corresponding author. Fax: +886-6-238-9940.
E-mail address: kcchang@mail.ncku.edu.tw (K.-C. Chang).

0017-9310/00/$ - see front matter
PII: S0017-9310(99)00177-5

Nomenclature

C_1, C_2, C_3, C_4, C_μ	turbulence model coefficients
C_f	skin friction coefficient
c_p, c_v	specific heat capacities at constant pressure and at constant volume, respectively
D, E	model functions
e	internal energy
Ec	modified Eckert number; $=\lambda^*\frac{u_0^*}{c_p^* q_w^* H^*}$
f_t, f_2, f_2', f_t, f_{w1}, f_{w2}, f_μ	viscous damping functions
G_k	production rate of turbulent kinetic energy
H	channel height
h	enthalpy
k	turbulent kinetic energy
Nu	Nusselt number based on the hydraulic diameter
P, p	instantaneous and mean pressures, respectively
q_w	wall heat flux
R	universal constant
Re_{D_h}, Re_τ	Reynolds numbers based on the mean velocity and hydraulic diameter and on the friction velocity and height, respectively
T, t	instantaneous and mean temperatures, respectively
U, u, u_τ	instantaneous, mean, and friction velocities, respectively
y	normal distance from wall

Greek symbols

α	thermal diffusivity
β	coefficient of thermal expansion
δ_{ij}	Dirac delta function
ε	dissipation rate of turbulent kinetic energy
Θ, θ	Nondimensionalized forms of instantaneous and mean temperatures, respectively; $(\Theta = T^* - T_0^* q_w^* H^*/\lambda^*)$
λ	thermal conductivity
μ	viscosity; $=\frac{\mu^*}{\rho^* u_0^* H^*}$
ν	kinematic viscosity
ρ	density
σ, σ_t	molecular and turbulent Prandtl numbers, respectively
σ_k, σ_ε	turbulent diffusion coefficients for k and ε, respectively
τ_w	wall shear stress
Φ	viscous dissipation rate

Superscripts

$'$	fluctuation
*	dimensional property
$+$	normalized by the wall variables, q_w, u_τ, and ν
$-$	Reynolds averaging

Subscripts

b	bulk
cp, cv	at constant pressure and constant volume, respectively
p	first grid node from wall
eff	effective
t	eddy
w	wall
0	reference state

tacitly between turbulent momentum and heat transport. Also, the σ_t needs to be prescribed either as a constant value [3] or from an algebraic function of turbulent Peclet number [2].

An alternative approach to determine σ_t is to solve directly the transport equations for turbulent heat fluxes [4–6]. In particular, this approach works properly for the situations where the similarity between the velocity and temperature fields does not hold so that σ_t is far from constant in contrast to the situation in a simple boundary-layer flow where the velocity and temperature fields develop simultaneously. However, the near-wall turbulence models for the scalar (heat or mass) transport is still rather primitive as compared to those for the momentum transport (flow field).

In this work, a rigorous formulation of the Reynolds-averaged energy equation for gaseous media is revisited and compared to the one commonly adopted in the turbulent heat transfer analysis by the researchers. Special attention is placed on the situation when the Reynolds-averaged energy equation has to work with the LRN k–ε turbulence models in a channel flow problem.

2. Reynolds-averaged formulation

For the energy conservation without consideration of thermal radiation in a steady-state turbulent flow, the (thermal) energy equation can be expressed in terms of either internal energy or enthalpy, respectively, as follows [7].

$$\frac{\partial}{\partial x_j^*}\left(\rho^* U_j^* e^*\right) = \frac{\partial}{\partial x_j^*}\left(\lambda^* \frac{\partial T^*}{\partial x_j^*}\right) - P^* \frac{\partial U_j^*}{\partial x_j^*} + \mu^* \Phi^* \quad (3)$$

$$\frac{\partial}{\partial x_j^*}\left(\rho^* U_j^* h^*\right) = \frac{\partial}{\partial x_j^*}\left(\lambda^* \frac{\partial T^*}{\partial x_j^*}\right) + U_j^* \frac{\partial P^*}{\partial x_j^*} + \mu^* \Phi^* \quad (4)$$

where $h^* = e^* + p^*/\rho^*$. The viscous dissipation term $\mu^*\Phi^*$ is usually negligible for the low-Mach-number flows as to be investigated in this study. By use of the canonical relations for internal energy and enthalpy and the Maxwell's relations, the changes in internal energy and enthalpy are expressed, respectively, as [7]

$$\mathrm{d}e^* = c_v^* \,\mathrm{d}T^* - \frac{1}{\rho^{*2}}\left[T^*\left(\frac{\partial p^*}{\partial T^*}\right)_{\rho^*} - P^*\right]\mathrm{d}\rho^* \quad (5)$$

$$\mathrm{d}h^* = c_p^* \,\mathrm{d}T^* + \frac{1}{\rho^*}\left(1 - \beta^* T^*\right)\mathrm{d}P^* \quad (6)$$

where

$$\beta^* = -\frac{1}{\rho^*}\left(\frac{\partial \rho^*}{\partial T^*}\right)_{P^*} \quad (7)$$

Substitution of Eqs. (5) and (6) into Eqs. (3) and (4) yields

$$\frac{\partial}{\partial x_j^*}\left(\rho^* c_v^* U_j^* T^*\right) = \frac{\partial}{\partial x_j^*}\left(\lambda^* \frac{\partial T^*}{\partial x_j^*}\right) - T^*\left(\frac{\partial P^*}{\partial T^*}\right)_{\rho^*} \frac{\partial U_j^*}{\partial x_j^*} \quad (8)$$

$$\frac{\partial}{\partial x_j^*}\left(\rho^* c_p^* U_j^* T^*\right) = \frac{\partial}{\partial x_j^*}\left(\lambda^* \frac{\partial T^*}{\partial x_j^*}\right) + \beta^* T^* U_j^* \frac{\partial P^*}{\partial x_j^*} \quad (9)$$

which are two different forms in terms of temperature but mathematically equivalent equations of energy conservation for a pure substance. For the case of incompressible liquid, Eqs. (8) and (9) reduces to an identical form of

$$\frac{\partial}{\partial x_j^*}\left(\rho^* c^* U_j^* T^*\right) = \frac{\partial}{\partial x_j^*}\left(\lambda^* \frac{\partial T^*}{\partial x_j^*}\right) \quad (10)$$

while for the case of ideal gas (such as the most gaseous media under atmospheric pressure and room temperature), Eqs. (8) and (9) can be expressed, respectively, by

$$\frac{\partial}{\partial x_j^*}\left(\rho^* c_v^* U_j^* T^*\right) = \frac{\partial}{\partial x_j^*}\left(\lambda^* \frac{\partial T^*}{\partial x_j^*}\right) - P^* \frac{\partial U_j^*}{\partial x_j^*} \quad (11)$$

$$\frac{\partial}{\partial x_j^*}\left(\rho^* c_p^* U_j^* T^*\right) = \frac{\partial}{\partial x_j^*}\left(\lambda^* \frac{\partial T^*}{\partial x_j^*}\right) + U_j^* \frac{\partial P^*}{\partial x_j^*} \quad (12)$$

with

$$c_p^* = c_v^* + R^* \quad (13)$$

A further simplification can be made under the condition of small temperature variations (<20 K, which were the test conditions in many convective heat transfer studies), that is, the specific heat capacities, thermal conductivity, and density can be approximately taken as constants. Incorporated with the assumptions, Eqs. (11) and (12) can be rewritten, respectively, in dimensionless form of

$$\frac{\partial}{\partial x_j}\left(\rho U_j \Theta\right) = \frac{\partial}{\partial x_j}\left(\frac{\mu}{\sigma_{\mathrm{cv}}} \frac{\partial \Theta}{\partial x_j}\right) \quad (14)$$

$$\frac{\partial}{\partial x_j}\left(\rho U_j \Theta\right) = \frac{\partial}{\partial x_j}\left(\frac{\mu}{\sigma_{\mathrm{cp}}} \frac{\partial \Theta}{\partial x_j}\right) + Ec \frac{\partial}{\partial x_j}\left(P U_j\right) \quad (15)$$

where σ_{cv} and σ_{cp} are the molecular Prandtl numbers defined by the specific heat capacities at constant volume and at constant pressure, respectively.

The Reynolds-averaged continuity and momentum equations are given by

$$\frac{\partial u_j}{\partial x_j} = 0 \quad (16)$$

$$\frac{\partial}{\partial x_j}(\rho u_j u_i) = -\frac{\partial p}{\partial x_j} + \frac{\partial}{\partial x_j}\left[\mu\left(\frac{\partial u_i}{\partial x_j} + \frac{\partial u_j}{\partial x_i}\right)\right] - \frac{\partial}{\partial x_j}\left(\rho \overline{u_i' u_j'}\right) \quad (17)$$

while the Reynolds-averaged energy equation can be written in either form of

$$\frac{\partial}{\partial x_j}\left(\rho u_j \theta\right) = \frac{\partial}{\partial x_j}\left(\frac{\mu}{\sigma_{\mathrm{cv}}} \frac{\partial \theta}{\partial x_j}\right) - \frac{\partial}{\partial x_j}\left(\rho \overline{u_j' \theta'}\right) \quad (18)$$

or

$$\frac{\partial}{\partial x_j}\left(\rho u_j \theta\right) = \frac{\partial}{\partial x_j}\left(\frac{\mu}{\sigma_{\mathrm{cp}}} \frac{\partial \theta}{\partial x_j}\right) + Ec \frac{\partial}{\partial x_j}(p u_j) - \frac{\partial}{\partial x_j}\left(\rho \overline{u_j' \theta'}\right) + Ec \frac{\partial}{\partial x_j}\left(\overline{p' u_j'}\right) \quad (19)$$

In Eqs. (17) and (18), two unknown correlations, i.e. Reynolds stress $\overline{u_i' u_j'}$ and the turbulent heat flux $\overline{u_j' \theta'}$ appear and they are generally modeled by using the classical Boussinesq approximation for the eddy diffusivity for momentum ν_t:

Table 1
Summary of coefficients and model functions[a]

Models	D	E	ε_w	σ_k	σ_ε	C_1	C_2
MK [16]	0	0	$\nu(\frac{\partial^2 k}{\partial y^2})$	1.4	1.3	1.4	1.8
NS [14]	$\max[-\frac{\nu}{2}\frac{\partial}{\partial y}(f_{w1}\frac{k}{\varepsilon}\frac{\partial \varepsilon}{\partial y}),0]$	$f_{w2}\nu\nu_t(\frac{\partial^2 u}{\partial y^2})^2+C_3\nu\frac{k}{\varepsilon}\frac{\partial k}{\partial y}\frac{\partial u}{\partial y}\frac{\partial^2 u}{\partial y^2}+C_4\nu\frac{\partial}{\partial y}[f_{w1}(1-f_{w1})\frac{\varepsilon}{k}\frac{\partial k}{\partial y}]$	$2\nu(\partial\sqrt{k}/\partial y)^2$	$1.2/f_t$	$1.3/f_t$	1.45	1.9

[a] $C_\mu = 0.09$, $C_3 = 0.005$, $C_4 = 0.5$, $f_t = 1 + 3.5\exp[-(0.01R_t)^{3/4}]$.

$$\overline{-u_i'u_j'} = \nu_t\left(\frac{\partial u_i}{\partial x_j}+\frac{\partial u_j}{\partial x_i}\right)-\frac{2}{3}\delta_{ij}k \tag{20}$$

and by Eq. (1) for the eddy diffusivity for heat α_t, in the flows possessing low level of anisotropy. Nevertheless, if we choose the other set of equations, i.e. Eqs. (17) and (19) in the formulation, one more unknown correlation $\overline{p'u_j'}$ in addition to $\overline{u_i'u_j'}$ and $\overline{u_j'\theta'}$ are needed to be modeled. There exists another extra term, $Ec\frac{\partial}{\partial x_j}(pu_j)$, in the Reynolds-averaged energy equation written in terms of σ_{cp} as compared to the one in terms of σ_{cv}. However, it is found that the Reynolds-averaged energy equation adopted in most of the published papers [1,5,6,8] is in form of

$$\frac{\partial}{\partial x_j}(\rho u_j\theta) = \frac{\partial}{\partial x_j}\left(\frac{\mu}{\sigma_{cp}}\frac{\partial\theta}{\partial x_j}\right)-\frac{\partial}{\partial x_j}\left(\rho\overline{u_j'\theta'}\right) \tag{21}$$

in which the terms of $Ec\frac{\partial}{\partial x_j}(pu_j)$ and $Ec\frac{\partial}{\partial x_j}(\overline{p'u_j'})$, compared to Eq. (19), are ignored. This leads to a contradiction that the Reynolds-averaged energy equation can be given in the same form but expressed in terms either of σ_{cv}, Eq. (18), or of σ_{cp}, Eq. (21), for the ideal gaseous media.

The cause why Eq. (21), instead of Eq. (18) or Eq. (19), was so commonly used in the studies of convective heat transfer by the researchers comes from the following approximation. As typically argued by Schlichting [9], the work of compression and that due to friction, i.e. the last term in the right-hand side of Eq. (15), become important for the calculation of the temperature field when the free-stream (reference) velocity is comparable with that of sound, and when the equivalent temperature difference $(= q_w^* H^*/\lambda^*)$ becomes of the order of the absolute temperature of the free stream (T_0^*). This occurs in practice in the high-speed flight of vehicles at very high altitudes; otherwise, the term of $Ec\frac{\partial}{\partial x_j}(PU_j)$ is usually negligible in the calculation of the temperature field.

Nevertheless, the Reynolds-averaged process of $\frac{\partial}{\partial x_j}(PU_j)$ yields two terms: $\frac{\partial}{\partial x_j}(pu_j)$ and $\frac{\partial}{\partial x_j}(\overline{p'u_j'})$. The result in our study, which will be presented later, corroborated the above argument, that is, the temperature fields predicted with and without consideration of the $Ec\frac{\partial}{\partial x_j}(pu_j)$ term indeed differed slightly for the low-Mach-number flows investigated in the study. In contrast, the pressure diffusion term, $\frac{\partial}{\partial x_j}(\overline{p'u_j'})$, cannot be negligible in the near-wall region of the flow field [10,11]. The pressure diffusion term is also appeared in the formulation of the transport equation of turbulent kinetic energy (k) [12]. As shown in the computed budget of the pressure diffusion term from the DNS data of a turbulent channel flow with low Reynolds number [13], the profile of the pressure diffusion term reaches a maximum in the region very close to the wall (see Fig. 5 of [13]). Although the DNS data [13] reveals that the pressure diffusion term is small compared to the other terms in the transport equation of k, very close to the wall the pressure diffusion term is of the same order as the difference between the dissipation rate and the viscous-diffusion rate of k, which are the two dominant terms in the near-wall region, and has to be considered in modeling the near-wall turbulence closure for k [14,15]. Following this argument, exclusion of the pressure diffusion term as done in Eq. (21) is questionable in the near-wall region and this will be justified later.

3. Near-wall turbulence models

Extensive research efforts have been made in development of the near-wall turbulence closure models, including the LRN versions of the two-equation k–ε models and of the second-order Reynolds stress models, for predictions of wall-bounded shear flows in the past two decades. Since the LRN Reynolds stress models are much complex mathematically than the LRN k–ε models and the flow problem to be tested is a simple channel flow, two LRN versions of the k–ε models developed by Myong and Kasagi [16] and by Nagano and Shimada [14] (hereinafter referred as the MK and NS models, respectively) are selected in the present calculations for demonstration. Between them, the MK was the one out of the nine LRN k–ε models (excluding the NS model) investigated by Hrenya and coworkers who yielded the best overall performances in predicting turbulent pipe flows with [1] and without [17] heat transfer, while the NS model which was developed from the direct-numerical-simulation (DNS) data of the detailed near-wall flow structure of the benchmark flow considers the pressure diffusion effects

Table 2
Summary of the viscous damping functions[a]

Models	f_μ	f_1	f_2
MK [16]	$[1-\exp(-\frac{y^+}{70})](1+\frac{3.45}{R_t^{1/2}})$	1	$\{1-\frac{2}{9}\exp[-(\frac{R_t}{6})^2]\}[1-\exp(-\frac{y^+}{5})]^2$
NS [14]	$(1-f_{w2})\{1+\frac{45}{R_t^{3/4}}\exp[-(\frac{R_t}{55})^{1/2}]\}$	1	$(1+f_2')(1-f_{w1})$

[a] $f_2=\exp(-2\times10^{-4}R^{13})[1-\exp(-2.2R^{1/2})]$, $f_{w1}=\exp[-(\frac{y^+}{9})^2]$, $f_{w2}=\exp[-(\frac{y^+}{44})^2]$, $R=\frac{k}{\varepsilon}[u_\tau^2/(\nu+\nu_t)](\frac{1}{R_t^{1/2}})f_{w1}$, $R_t=\frac{k^2}{\nu\varepsilon}$, $y^+=u_\tau y/\nu$, $u_\tau=(\frac{\tau_w}{\rho})^{1/2}$.

in the formulation of k and ε transport equations (D and E terms, respectively, see Table 1).

The general forms of the transport equations for the turbulent kinetic energy and its dissipation rate are

$$\frac{\partial}{\partial x_j}(\rho u_j k)=\frac{\partial}{\partial x_j}\left[\left(\mu+\frac{\mu_t}{\sigma_k}\right)\frac{\partial k}{\partial x_j}\right]+G_k-\rho\varepsilon+D \quad (22)$$

$$\frac{\partial}{\partial x_j}(\rho u_j\varepsilon)=\frac{\partial}{\partial x_j}\left[\left(\mu+\frac{\mu_t}{\sigma_\varepsilon}\right)\frac{\partial\varepsilon}{\partial x_j}\right]+(C_1f_1G_k-C_2f_2\rho\varepsilon)\frac{\varepsilon}{k}+E \quad (23)$$

where the production term G_k and the eddy viscosity μ_t are expressed, respectively, as

$$G_k=2\mu_t\frac{\partial u_i}{\partial x_j}\frac{\partial u_i}{\partial x_j} \quad (24)$$

$$\mu_t=\rho C_\mu f_\mu\frac{k^2}{\varepsilon} \quad (25)$$

The coefficients and the model functions shown in Eqs. (22)–(25) for the two tested turbulence models are summarized in Tables 1 and 2.

4. Test problem and numerical aspects

Test problem is the parallel-plate channel air flow with constant wall heat flux. Uniform mean streamwise and zero mean transverse velocity profiles as well as uniform mean temperature profile are assigned at the inlet. The inlet profiles of k and ε are given in the following empirical manner:

$$k=0.03u^2 \qquad \text{and} \qquad \varepsilon=C_\mu\frac{k^{3/2}}{0.03H} \quad (26)$$

Length of computational domain is extended to $40H$ which assures the flow with the specified inlet conditions being fully developed. The fully-developed condition of temperature for the case of constant wall heat flux is $\partial^2\theta/\partial x^2=0$. At the symmetric centerline, the zero-gradient condition is met except for $\nu=0$. At the solid wall, all quantities vanish except for ε_w, which is specified in Table 1, and θ_w. The wall heat flux is defined by

$$q_w^*=-\lambda_{eff}^*\left.\frac{\partial t^*}{\partial y^*}\right|_w \quad (27)$$

with

$$\lambda_{eff}^*=c_m^*\mu^*\left(\frac{1}{\sigma_m}+\frac{\mu_t}{\sigma_t}\right) \quad (28)$$

where m = cp or cv depending on the definition of the molecular Prandtl number. A constant value of $\sigma_t=0.9$ [18] is chosen for the calculations with the present boundary-layer flow. Nondimensionalization of Eq. (27) yields

$$\left.\frac{\partial\theta}{\partial y}\right|_w=-\left[1+\mu_t\left(\frac{\sigma_m}{\sigma_t}\right)\right]^{-1} \quad (29)$$

However, if the first grid node is placed in the immediate vicinity (viscous sublayer) of the wall, $\mu_t\to0$ and the term in the bracket of Eq. (29), then, approaches unity value.

Grid mesh used for the computational domain consists of 80×80 (streamwise by transverse) nonuniformly distributed grid nodes. To ensure the resolution of the near-wall region, about half of the grid nodes are placed within $y^+=50$ and the first grid node from the wall was placed at $y^+=O(10^{-1})$.

Solutions of the governing equations are obtained by the finite-volume method incorporated with the orthodox QUICK scheme [19] and the SIMPLEC algorithm with nonstaggered grid system [20]. The computed solution is assumed to have converged when the magnitude of the absolute residuals of momentum and energy, normalized by their respective inlet fluxes, falls below 10^{-5}.

5. Results and discussion

To clarify our doubt that the Reynolds-averaged energy equation, (21), which were commonly used in

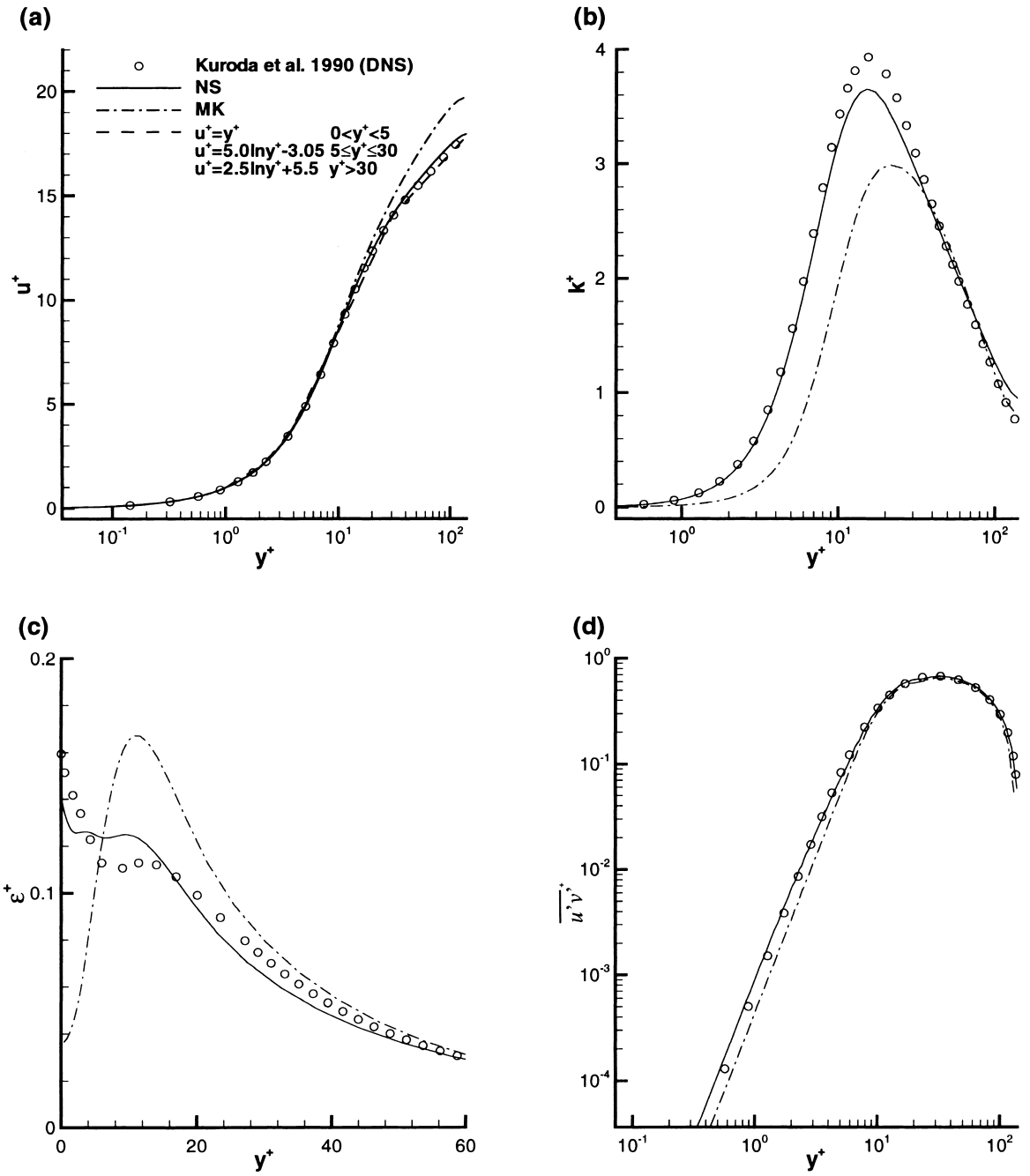

Fig. 1. Profiles of (a) mean streamwise velocity, (b) turbulent kinetic energy, (c) dissipation rate of turbulent kinetic energy, and (d) the Reynolds shear stress obtained with the two test models at $Re_\tau = 150$.

the convective heat transfer studies, might be overapproximated when working with the near-wall turbulence models, this equation and the one of the less approximated forms of the energy equation, (18), are separately solved for the temperature distributions of the test cases. Note that the only difference existed between Eqs. (18) and(21) is the definition of the molecular diffusion coefficient in terms of either σ_{cv}, or σ_{cp} respectively. Constant air density is assumed in the calculations since the temperature variations of the test

Table 3
Comparison of the predicted skin friction coefficients ($\times 10^3$)

Re_τ	MK model	NS model	DNS data	Dean's correlation, Eq. (30)
395	6.06	6.37	6.60 [22]	6.74
150	7.38	8.47	8.58 [23]	8.87[a]

[a] The Re_{D_h} value of 9160 ($Re_\tau = 150$) is beyond the applicable bounds of Eq. (30).

cases are small (less than 20 K) With this assumption, the solution of the flow field is thus decoupled with the solution of the thermal field, i.e., is independent of the choice of σ_{cv} or σ_{cp} in the Reynolds-averaged energy equation.

Calculations with the two test models are performed for the two benchmark cases with $Re_{D_h} = 27{,}500$ ($Re_\tau = 395$) and $Re_{D_h} = 9{,}160$ ($Re_\tau = 150$), respectively, since the detailed turbulence quantities are available from the DNS database [13,21,22] and [23,24], respectively.

The normalized profiles of the mean streamwise velocity, the turbulent kinetic energy and its dissipation rate, and the Reynolds shear stress obtained with the both test turbulence models are shown as a function of $y^+(= u_\tau^* y^*/\nu^*)$ and compared with the available DNS data [23] in Fig. 1 for the case of $Re_\tau = 150$. The experimental correlations based on the law of the wall are also included in Fig. 1a for further comparison with the predictions. It is clear that the turbulence quantities predicted with the NS model are in better agreement with the DNS data and the experimental correlations than what obtained with the MK model. In particular, the NS model gives qualitatively and quantitatively more exact predictions for the near-wall profile of ε than what the MK model does. Similar observation can be made for the case of $Re_\tau = 395$. However, detailed comparison between the model predictions and the DNS data for the case of $Re_\tau = 395$ can be found in the paper of Nagano and Shimada [15]. The results for the case of $Re_\tau = 395$ predicted with the two test turbulence models are not presented here for reasons of brevity. Table 3 collects the skin friction coefficients for the two test cases predicted with the MK and NS models and compares them with the DNS data and the experimental correlations computed from the empirical formula of Dean [25]:

$$C_f = 0.0868 Re_{D_h}^{-0.25}, \quad 1.2 \times 10^4 < Re_{D_h} < 1.2 \times 10^6 \tag{30}$$

Note that the Re_{D_h} value of 9160 for the flow at $Re_\tau = 150$ is rather low and beyond the applicable bounds of Dean's formula. However, its C_f value evaluated from Eq. (30) is also listed in Table 3 for reference. It can be concluded, based on all the above comparison, that the NS model, which considers the pressure diffusion effects in the near-wall turbulence modeling, provides better fits to the DNS data and to the law of the wall and consequently predicts the skin friction coefficients more accurately, as compared to the MK model.

Fig. 2 compares the predictions of $t^+ (= \rho^* c_p^* (t_w^* - t^*) u_\tau^* / q_w^*)$ obtained separately with the NS and MK models by used of either Eq. (18) or Eq. (21) for the two test cases. The experimental correlations made by Kader [26] are included in Fig. 2 for the purpose of comparison. Only the DNS data of thermal field at $Re_\tau = 150$ are available [24]. These DNS data are also presented in Fig. 2a and b. The results reveal that the t^+ predictions using Eq. (21) are lower than those using Eq. (18) particularly in the region with about $y^+ > 10$ for both of the tested turbulence models. Furthermore, the NS model incorporated with Eq. (18) which is a less approximated form of the Reynolds-averaged energy equation, compared to Eq. (21), provides the best fit to either the DNS data of Kasagi et al. [24] or the experimental correlations of Kader [26].

Tables 4 and 5 collect the Nusselt numbers predicted from the two tested turbulence models either with Eq. (18) or Eq. (21) for the cases at $Re_{D_h} = 395$ and 150,

Table 4
Comparison of the predicted Nusselt numbers at $Re_\tau = 395$[a]

Model	Eq. (18)	Eq. (21)	Eq. (21) with the $\Pi \frac{\partial}{\partial x_j}(pu_j)$ term
NS	62.49	73.75	74.10
MK	57.96	69.10	69.41

[a] Gnielinski's correlation, Eqs. (33) and (34): 65.95.

Table 5
Comparison of the predicted Nusselt numbers at $Re_\tau = 150$[a]

Model	Eq. (18)	Eq. (21)
NS	27.93	31.82
MK	25.20	28.50

[a] Gnielinski's correlation, Eqs. (33) and (34): 27.78 (the Re_{D_h} value of 9.160 for the present case is slightly beyond the applicable bounds of Eqs. (33) and (34)); DNS [24]: 30.8.

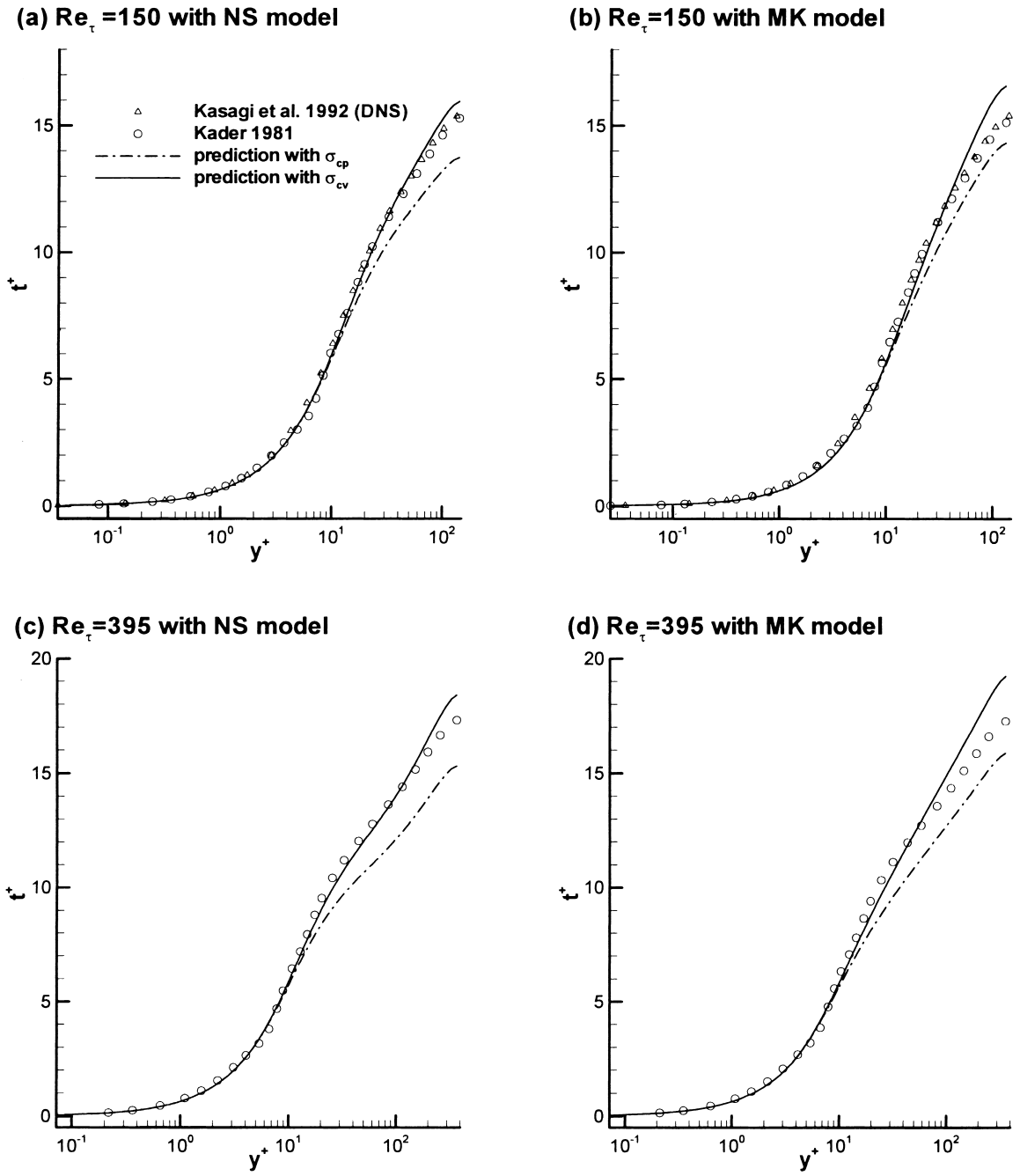

Fig. 2. Temperature distributions obtained respectively with the NS and MK models for the two test cases.

respectively. Here the Nusselt number is determined as follows. According to Newton's law of cooling:

$$q_w^* = h^*\left(t_w^* - t_b^*\right) \tag{31}$$

Through the relationships of Eqs. (27) and (28), the Nu can be expressed in the dimensionless form of

$$Nu = \left(1 + \mu_t \frac{\sigma_m}{\sigma_t}\right) \frac{t_p^+}{t_b^+} \frac{1}{y_p} \tag{32}$$

where m = cp or cv depending on the definition of the molecular Prandtl number; and y_p denotes the normal distance of the first grid node from the wall. The Nu values evaluated from the empirical formula of

Gnielinski [27],

$$Nu = \frac{\left(Re_{D_h} - 1000\right)\sigma_{cp}(f/8)}{1 + 12.7(f/8)^{1/2}\left(\sigma_{cp}^{2/3} - 1\right)} \tag{33}$$

where

$$f = \left(0.79 \ln Re_{D_h} - 1.64\right)^{-2}, \quad 10^4 < Re_{D_h} < 5 \times 10^6 \tag{34}$$

are also listed in Tables 4 and 5. The trend in the Nu prediction shown in Tables 4 and 5 is consistent with what was observed for the C_f prediction (see Table 3), i.e., the predictions using the MK model are below the predictions using the NS model. Furthermore, the Nu values predicted with Eq. (21) for both the test models are $18.6 \pm 0.6\%$ and $13.5 \pm 0.4\%$ higher than those predicted with Eq. (18) for the cases of $Re_\tau = 395$ and 150, respectively. Comparisons made in Tables 4 and 5 indicate that the predictions using the NS model worked with Eq. (18) provide the closest agreement with the experimental correlations of Gniclinski [27]. This conclusion deems reasonable because the NS model has been proven to be able to yield better predictions of the turbulent flow structure than the MK model. In addition, Eq. (18) is a more rigorous form of the energy equation than Eq. (21).

However, the Nu value (30.8) at $Re_\tau = 150$ obtained from the DNS calculation of Kasagi et al. [24] somewhat deviates from (about 11% higher) the Gnielinski's correlation ($N = 27.27$). It should be noted that the Re_{D_h} of 9,160 for the case at $Re_\tau = 150$ is slightly beyond the lower bound (10^4) of Gnielinski's formula. It is worthwhile to understand why the temperature distribution of the DNS data (see Fig. 2a) is in good agreement with the experimental correlations made by Kader [26], whereas the Nu values determined from the DNS data is overpredicted than from the experimental correlations made by Gnielinski [27]. In the DNS calculation of Kasagi et al. [24], they adopted the energy equation in the form of Eq. (15) but dropped the term of $Ec\frac{\partial}{\partial x_j}(PU_j)$ due to the usual approximation for the low-Mach-number flow. The corresponding Reynolds-averaged energy equation is the same as Eq. (21). However, the comparisons made from Fig. 3 and Table 5 revealed that the temperature profile predicted with Eq. (21) is apparently lower than that of DNS calculation except in the very near-wall region ($y^+ < 1$), whereas their Nu values agree well each other but both are higher than the Gnielinski's correlation. As pointed out before, the differences between Eqs. (21) and (19) are the absence of two terms of $Ec\frac{\partial}{\partial x_j}(pu_j)$ and $Ec\frac{\partial}{\partial x_j}(\overline{p'u_j'})$. In order to examine which dismissed term plays more important role resulting in the observed discrepancies of the temperature and Nu predictions, the calculations using Eq. (21) with the ad-

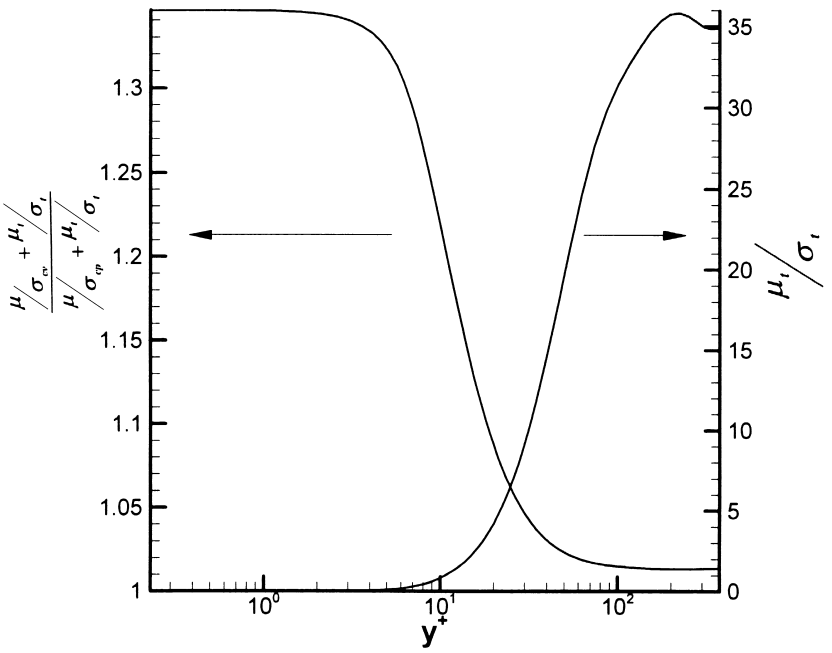

Fig. 3. Variations of the ratio of the effective diffusion coefficient used in Eq. (18) to the one in Eq. (21) and of μ_t/σ_t versus y^+ at $Re_\tau = 395$.

ditional $Ec\frac{\partial}{\partial x_j}(pu_j)$ term are implemented for the case of $Re_\tau = 395$ and their predicted Nu results are listed in Table 4 too. Comparison between the Nu predictions using Eq. (21) with and without the $Ec\frac{\partial}{\partial x_j}(pu_j)$ term reveals that the inclusion of the $Ec\frac{\partial}{\partial x_j}(pu_j)$ term in the Reynolds-averaged energy equations affect slightly the Nu predictions for both the test turbulence models. Similar observation is obtained from the comparison between the predicted temperature distributions using Eq. (21) with and without the $Ec\frac{\partial}{\partial x_j}(pu_j)$ term which are not presented here for reasons of brevity. It implies that exclusion of the pressure gradient term in the Reynolds-averaged formulation of the energy equation as done in Eq. (21) is the main reason resulting in erroneous predictions of the temperature distribution and the Nusselt number compared to what obtained with Eq. (18). However, the study on the budget of the pressure diffusion term in the DNS calculation [13] revealed that this term has to be taken into account in the region very close to the wall, and its contribution can be negligible in the other region of the flow field. A conclusion can thus be drawn as follows. The usual approximation which neglects the work of compression and that due to friction in the energy equation, (15), is valid except in the very near-wall region where the advective effect becomes small due to the no-slip condition at the wall. This, then, explains the present comparison results between the DNS data and the experimental correlations, that is, well agreement in the temperature profile but overestimation in the Nusselt number. Further corroboration of this inference can be done by repeating DNS calculation using either Eq. (14) or Eq. (15) but without neglecting the $Ec\frac{\partial}{\partial x_j}(PU_j)$ term, and it remains to be studied in the future.

It has been demonstrated that, when solved by the Reynolds-averaged formulation along with the low-Reynolds-number k–ε models, the choice of either Eq. (18) or Eq. (21) to serve as the energy equation did yield remarkable differences in the predictions of the temperature distribution and the Nusselt number. To look inside how the different definitions of the molecular Prandtl number used in Eqs. (18) and (21) affects the simulation result, Fig. 3 which records variations of the ratio of the effective diffusion coefficient, $\mu/\sigma + \mu_t/\sigma_t$, used in Eq. (18) to the one in Eq. (21) and of μ_t/σ_t in the flow field for the case of $Re_\tau = 395$ is presented. As shown in Fig. 3, μ_t approaches zero value in the vicinity of the wall where the inertia terms of the Reynolds-averaged equations of momentum and energy become small due to the no-slip condition imposed on the wall (see Fig. 1a) while the diffusion terms become dominant. It leads to the result of Fig. 3 that the molecular diffusion coefficient, μ/σ, plays more dominant role, as the transverse position y is moved closer to the wall, in the determination of the

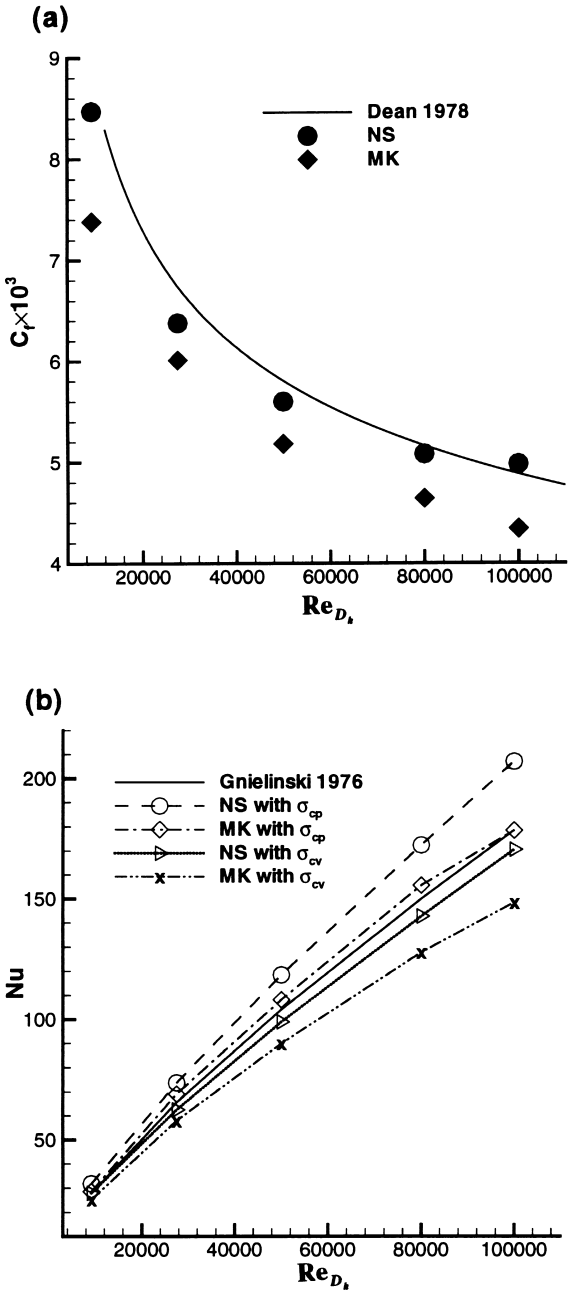

Fig. 4. Comparison between the experimental correlations and the predictions of (a) skin friction coefficients and (b) Nusselt numbers using the two test models at different levels of Reynolds number.

effective diffusion coefficient. It is agreed that the use of the low-Reynolds-number turbulence models requires a number of grid nodes being placed in the near-wall region. For example, approximate 40 grid nodes were placed in the region within $y^+ = 50$ and the first grid node was at $y^+ = O(10^{-1})$, where $\mu_t \ll \mu$

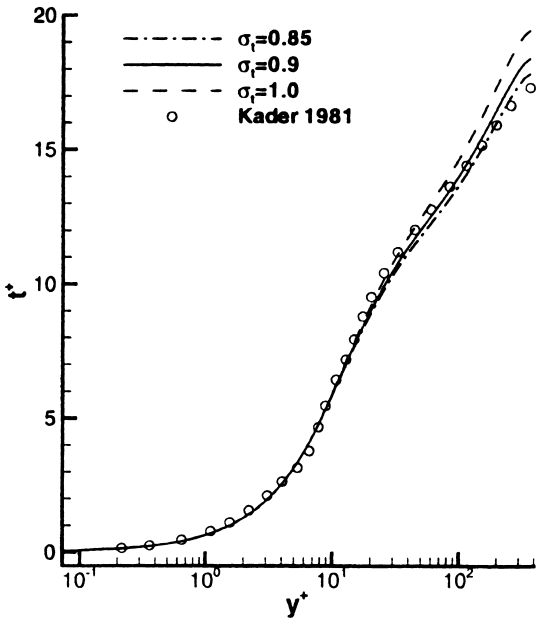

Fig. 5. Effect of σ_t on temperature distribution at $Re_\tau = 395$ using the NS model and Eq. (18).

in the present calculations. Nevertheless, the result of Fig. 3 shows that the use of σ_{cv} or σ_{cp} does affect the values of the effective diffusion coefficient in this near-wall region for the thermal field calculation incorporated with the LRN k–ε turbulence models. In contrast, the conventional wall-function approach which bridges the conditions at the wall to the fully turbulent flow zone and permits to use coarse grid density in the near-wall region is insensitive to the value used for σ in the calculations, because the first grid node from the wall must be placed in the region of $y_p > 11.6$ to apply for the law of the wall [7] where μ_t/σ_t, becomes dominant as shown in Fig. 3. This could explain why the overapproximation made in Eq. (21) does not cause remarkable errors in the thermal field calculations using the wall-function approach.

It has to be noted that the DNS data selected for the present comparisons were carried out at very low Reynolds numbers which are beyond most of engineering interest. It will be instructive to compare the experimental correlations with what would be predicted with either Eq. (18) or Eq. (21) at higher Reynolds numbers. Fig. 4 shows predicted C_fs and Nus at different levels of Re_{D_h} together with the relevant experimental correlations. It is concluded once more that the NS model is superior to the MK model as far as the ability to predict C_f is concerned, while the NS model worked with Eq. (18) is capable of yielding satisfactory Nu predictions as compared to the Gnielinski's correlations. It is interesting to note that the MK model worked with Eq. (21) which is an overapproximated form of the Reynolds-averaged energy equation happens to yield good Nu predictions as reported in the study of Hrenya et al. [1].

The effective diffusion coefficient appeared in the Reynolds-averaged energy equation is composed of μ/σ and μ_t/σ_t. It can be expected that Nu and the t^+ profile are also influenced by, except σ value, the ability of the turbulence model to predict μ_t in the near-wall region and the value selected for σ_t. Fig. 5 shows a typical effect of σ_t on the temperature distribution at $Re_\tau = 395$. The NS model worked with Eq. (18) is used for the demonstration since this turbulence model has been shown to have better ability to predict near-wall flow structure accurately. The calculated discrepancies of Nus from the Gnielinski's correlation (see Table 4) with $\sigma_t = 0.85$, 0.9 (selected for the present work), and 1.0 are −9.6, −4.9, and −2.2%, respectively. The study for the case of $Re_\tau = 395$ shows that increasing σ_τ, pushes the t^+ profile higher than data of Kader [26], which moves Nu closer to the Gnielinski's correlation. It indicates that the value selected for σ_t affects the solution of the thermal field to a certain extent. The profile of σ_t in the near-wall region has been a matter of conjecture; for example, Kays [28] examined σ_t variation in the two-dimensional, fully developed flow using the presently available experimental and DNS data. He attempted to find some correlations of σ_t in terms of turbulent Peclet number and y^+ for whole range of Prandtl number. However, Kays adopted Eq. (21), which has been shown as an overapproximated form of the Reynolds-averaged energy equation, in the heat transfer analysis including gaseous media; consequently, part of his conclusions drawn in Ref. [28] has to be re-examined and remains to be studied further using a rigorous form of the Reynolds-averaged energy equation for gaseous media.

6. Conclusions

The Reynolds-averaged energy equation used with the LRN k–ε models is revisited. It is shown that Eq. (21) which was so commonly used in theoretical studies of the turbulent heat transfer for gaseous media yields remarkable deviations in the thermal field prediction particularly for Nusselt number, mainly due to the overapproximation by dropping the pressure diffusion term in it. Eq. (18), which is one of the rigorous forms of the Reynolds-averaged energy equation in terms of temperature and free of the unknown correlation $\overline{p'u'_j}$, is suggested to be used in the formulation of the turbulent heat transfer for gaseous media when working with the near-wall turbulence closure models.

Acknowledgements

The authors gratefully acknowledge the grant support from the National Science Council of the Republic of China under the contract NSC88-2212-E006-037.

References

[1] C. Hrenya, S. Miller, T. Mallo, J. Sinclair, Comparison of low Reynolds number k–ε turbulence models in predicting heat transfer rates for pipe flow, International Journal of Heat and Mass Transfer 41 (1998) 1543–1547.

[2] W. Kays, M. Crawford, in: Convective Heat and Mass Transfer, 3rd ed., McGraw-Hill, New York, 1993, p. 267.

[3] K.C. Chang, Y. Yamanaka, W.D. Hsieh, Examination of wall boundary condition for dissipation rate of turbulence energy in numerical calculation with low-Reynolds-number k–ε models, in: Proceedings of International Conference on Fluid Engineering, Vol. 3, Tokyo, Japan, 1997, pp. 1157–1162.

[4] R.M.C. So, T.P. Sommer, A near-wall eddy conductivity model for fluids with different Prandtl numbers, ASME Journal of Heat Transfer 116 (1994) 844–854.

[5] K. Abe, T. Kondoh, Y. Nagano, A new turbulence model for predicting fluid flow and heat transfer in separating and reattaching flows — II. Thermal field calculations, International Journal of Heat and Mass Transfer 38 (1995) 1467–1481.

[6] Y. Nagano, M. Shimada, Development of a two-equation heat transfer model based on direct simulations of turbulent flows with different Prandtl numbers, Physics of Fluids 8 (1996) 3379–3402.

[7] A. Bejan, Convection Heat Transfer, 2nd ed., Wiley, New York, 1995, pp. 9–15, 298, 305.

[8] Y. Nagano, C. Kim, A two-equation model for heat transport in wall turbulent shear flows, ASME Journal of Heat Transfer 110 (1988) 583–589.

[9] H. Schlichting, Boundary Layer Theory, 7th ed., McGraw-Hill, New York, 1979, pp. 272–274.

[10] J. Kim, On the structure of pressure fluctuations in simulated turbulent channel flow, Journal of Fluid Mechanics 205 (1989) 421–451.

[11] C. Wark, A. Naguib, W. de Ojeda, O. Juckenhoefel, On the relationship between the wall pressure and velocity field in a turbulent boundary layer, in: 29th AIAA Fluid Dynamics Conference, AIAA 98-2642, Albuquerque, NM, 1998.

[12] D.C. Wilcox, Turbulence Modeling for CFD, DCW Industries, La Canada, CA, 1993, p. 74.

[13] N.N. Mansour, J. Kim, P. Moin, Reynolds-stress and dissipation-rate budgets in a turbulent channel flow, Journal of Fluid Mechanics 194 (1988) 15–44.

[14] Y. Nagano, M. Shimada, Rigorous modeling of dissipation-rate equation using direct simulation, JSME International Journal Series B 38 (1995) 51–59.

[15] C.B. Hwang, C.A. Lin, Improved low-Reynolds-number k–ε model based on direct-numerical simulation data, AIAA Journal 36 (1998) 38–43.

[16] H.K. Myong, N. Kasagi, A new approach to the improvement of k–ε turbulence model for wall-bounded shear flows, JSME International Journal, Series II 33 (1990) 63–72.

[17] C.M. Hrenya, E.J. Bolio, D. Chakrabarti, J.L. Sinclair, Comparison of low Reynolds number turbulence models in predicting fully developed pipe flow, Chemical Engineering Science 50 (1995) 1923–1941.

[18] W.P. Jones, B.E. Launder, The calculation of low-Reynolds-number phenomena with a two-equation model of turbulence, International Journal of Heat and Mass Transfer 16 (1973) 1119–1130.

[19] W.D. Hsieh, K.C. Chang, Turbulent flow calculation with orthodox QUICK scheme, Numerical Heat Transfer, Part A 30 (1996) 589–604.

[20] T.F. Miller, F.W. Schmidt, Use of a pressure-weighted interpolation method for the solution of incompressible Navier–Stokes equation on a nonstaggered grid system, Numerical Heat Transfer 14 (1988) 213–233.

[21] J. Kim, P. Moin, R. Moser, Turbulence statistics in fully developed channel flow at low-Reynolds-number, Journal of Fluid Mechanics 177 (1987) 133–166.

[22] J. Kim, Collaborative testing of turbulence models (organized by P. Bradshaw, B.E. Launder, and J.L. Lumley), Data Disk No. 4, 1990.

[23] K. Kuroda, Direct numerical simulation of turbulent Couette-Poiseuille flows. Ph.D. thesis, Department of Mechanical Engineering, The University of Tokyo, Tokyo, Japan, 1990.

[24] N. Kasagi, Y. Tomita, A. Kuroda, Direct numerical simulation of passive scalar field in a turbulent flow, ASME Journal of Heat Transfer 14 (1992) 598–606.

[25] R.B. Dean, Reynolds number dependence of skin friction and other bulk flow variables in two-dimensional rectangular duct flow, ASME Journal of Fluid Engineering 100 (1978) 215–223.

[26] B.A. Kader, Temperature and concentration profiles in fully turbulent boundary layers, International Journal of Heat and Mass Transfer 24 (1981) 1541–1544.

[27] V. Gnielinski, New equations for heat and mass transfer in turbulent pipe and channel flow, International Chemical Engineering 16 (1976) 359–368.

[28] W.M. Kays, Turbulent Prandtl number—where are we?, ASME Journal of Heat Transfer 116 (1994) 284–295.